1-1-1996

Site-Selective Excitation And Polarized Absorption Spectra Of Nd3+ In Sr-5(Po4)(3)F And Ca-5(Po4)(3)F

John B. Gruber

Clyde A. Morrison

Michael D. Seltzer

Andrew O. Wright

Melvin P. Nadler

See next page for additional authors

Site-selective excitation and polarized absorption spectra of Nd^{3+} in $Sr_5(PO_4)_3F$ and $Ca_5(PO_4)_3F$

Cite as: Journal of Applied Physics **79**, 1746 (1996); https://doi.org/10.1063/1.360964
Submitted: 25 July 1995 . Accepted: 13 October 1995 . Published Online: 17 August 1998

John B. Gruber, Clyde A. Morrison, Michael D. Seltzer, Andrew O. Wright, Melvin P. Nadler, Toomas H. Allik, J. Andrew Hutchinson, and Bruce H. T. Chai

Site-selective excitation and polarized absorption spectra of Nd^{3+} in $Sr_5(PO_4)_3F$ and $Ca_5(PO_4)_3F$

John B. Gruber
Department of Physics, San Jose State University, San Jose, California 95192-0106

Clyde A. Morrison
Army Research Laboratory, Adelphi, Maryland 20783-1145

Michael D. Seltzer, Andrew O. Wright, and Melvin P. Nadler
Naval Air Warfare Center Weapons Division, China Lake, California 93555-6001

Toomas H. Allik
Science Applications International Corporation, 1710 Goodridge Drive, McLean, Virginia 22102

J. Andrew Hutchinson
Night Vision and Electronics Sensors Directorate, U.S. Army, Fort Belvoir, Virginia 22060-5806

Bruce H. T. Chai
Center for Research on Electro-optics and Lasers, University of Central Florida, Orlando, Florida 32836

(Received 25 July 1995; accepted for publication 13 October 1995)

Polarized absorption and fluorescence spectra were analyzed to establish individual energy (Stark) levels of Nd^{3+} ions in host crystals of $Sr_5(PO_4)_3F$ (SFAP) and $Ca_5(PO_4)_3F$ (FAP). Site-selective excitation and fluorescence facilitated differentiation between Nd^{3+} ions in emitting sites associated with 1.06 μm stimulated emission, and nonemitting Nd^{3+} ions in other sites. Measurements were made on samples containing different concentrations of Nd^{3+} at 4 K and higher temperatures. Substitution of Nd^{3+} for Sr^{2+} or Ca^{2+} was accompanied by passive charge compensation during crystal growth. Crystal-field splitting calculations were performed according to site for Stark levels of Nd^{3+} ions identified spectroscopically. We obtained a final set of crystal-field parameters B_{nm} for Nd^{3+} ions in fluorescing sites with a rms. deviation of 7 cm^{-1} (52 levels in Nd:SFAP) and 8 cm^{-1} (59 levels in Nd:FAP). For one of the nonemitting sites in Nd:FAP we obtained a final set of B_{nm} parameters which gave a rms deviation of 6 cm^{-1} between 46 experimental and calculated levels. © *1996 American Institute of Physics.* [S0021-8979(96)01403-2]

INTRODUCTION

Fluorapatite crystals $Ca_5(PO_4)_3F$ (FAP), $Sr_5(PO_4)_3F$ (SFAP), and $Sr_5(VO_4)_3F$ (SVAP), containing trivalent rare-earth ions, have been grown recently with sufficiently favorable optical properties to warrant further study of their spectroscopy and evaluation of their laser performance.[1–8] The potential of these crystals as optical materials has been demonstrated by the efficient generation of stimulated emission at 1.04 μm in Yb:SVAP,[3,4,9] and by the successful use of Er:FAP as a saturable absorber for passive Q switching of an Er^{3+}-doped phosphate glass laser operating at 1.53 μm.[10–12] Interpretation of the Nd:FAP spectra has been of interest to a number of groups whose early studies (nearly 30 years ago) centered around the luminescence features of the crystal and its potential as a laser.[13–18] More recently, spectroscopy and laser performance studies show that Nd:SVAP has promise as a new laser source.[8]

The complex optical spectra attributed to rare-earth ions occupying numerous crystal-field environments is a general characteristic of the fluorapatite crystals grown with rare-earth ions as dopants.[6,7,11] Heterovalent substitution by rare-earth ions for Ca and Sr in two different positions in the hexagonal crystal lattice, M(I) and M(II), requires some form of charge compensation.[19–23] Possible charge-compensation mechanisms for R^{3+} ions in either or both host cation positions have been proposed by several groups.[16,23,24] The possible substitution of two types of lattice cations and the location of charge-compensating ions and defects, relative to the R^{3+} ions, accounts for variation in the crystal-field environment experienced by individual R^{3+} ions. The particular environment, or site, occupied by a R^{3+} ion has considerable influence over the optical behavior of that ion. For instance, some of the Nd^{3+} ions in these hosts do not emit radiation upon excitation, and therefore are not likely to contribute to laser action.[5,9,24] Furthermore, some appear to serve as quenching centers.[24] Indeed, this characteristic is most evident for FAP crystals in which Nd^{3+} ions appear to be distributed among both emitting and nonemitting sites. In SFAP, Nd^{3+} ions appear to occupy emitting sites predominantly.

Our purpose is to identify the details of the crystal-field splitting of the energy levels of Nd^{3+} ions that occupy both emitting and nonemitting sites in Nd:FAP and Nd:SFAP using site-selective excitation and polarized absorption as optical probes. This approach allows us to dissect complex absorption spectra and identify features which arise from Nd^{3+} ions in specific sites. We find that the spectra of Nd:SFAP have fewer absorption and emission lines than comparable

 0021-8979/96/79(3)/1746/13/$6.00

spectra observed for Nd:FAP. This suggests that the availability of optical centers for appreciable occupation by Nd^{3+} ions in SFAP is limited relative to FAP.

In the course of our ongoing investigation of R^{3+}-doped FAP and SFAP crystals, we have observed polarized absorption and fluorescence spectra for non-Kramers ions such as Eu^{3+} and Pr^{3+} consistent with selection rules associated with C_s symmetry.[6,7] In both FAP and SFAP, such polarization was observed for the principally occupied site, and therefore attributed to be M(II). Because Nd^{3+} is a Kramers ion, we have less direct evidence to suggest that Nd^{3+} prefers the M(II) location as well. However, resemblances between the spectra of Nd:SFAP and some of the features observed in the spectra of Nd:FAP, and similar comparisons made between other R:FAP and R:SFAP crystals, clearly indicate that the emitting Nd^{3+} ions in both FAP and SFAP occupy M(II) locations with C_s symmetry.[24] This hypothesis is consistent with the suggestion by other groups[15,16,18,23] that the laser-active R^{3+} ions in FAP and SFAP occupy M(II) locations with C_s symmetry.

In addition to spectral features attributed to the principally occupied sites in Nd:FAP we observe relatively weaker absorption lines which also polarize. Analysis of these spectra is consistent with selection rules operating for Nd^{3+} ions in sites having C_3 symmetry. Since no Nd^{3+} ion emission is observed for the site, we base this interpretation on the polarized absorption spectra reported in Table I. This site is one of several nonfluorescing sites described by Maksimova and Sobol'[15,16] who suggest that some Nd^{3+} ions may substitute into M(I) divalent cation sites. These sites have C_3 symmetry and represent 40% of all cation sites in the undoped lattice. They speculate that charge compensation for this site is sufficiently remote so that C_3 symmetry is preserved for Nd^{3+} ions in the site.[25]

Crystal-field splitting calculations were performed for Stark levels of Nd^{3+} ions in spectroscopically different sites. Using crystal-field parameters $B_{\rm nm}$ reported for Nd:SVAP as a starting set,[5] we obtained a final set for Nd^{3+} ions in fluorescing sites with a rms deviation of 7 cm^{-1} (52 levels in Nd:SFAP) and 8 cm^{-1} (59 levels in Nd:FAP). Peale *et al.*[5] obtained a rms of 6 cm^{-1} for 28 levels of Nd^{3+} in the emitting site in Nd:SVAP. Using B_{nm} parameters obtained from a lattice-sum calculation for Nd^{3+} ions in sites of C_3 symmetry, we obtained a final set of B_{nm} parameters which gave a rms of 6 cm^{-1} between 46 experimental and calculated levels for one of the nonemitting sites.

EXPERIMENTAL DETAILS

Boules of Nd:SFAP and Nd:FAP containing nominally 1 at. wt % neodymium, were grown by the standard Czochralski method at the University of Central Florida, CREOL. The hexagonal crystals were cut parallel and perpendicular to the crystalline optical axis (c axis). Crystals containing lesser quantities of Nd^{3+} ions were also examined spectroscopically. The actual amount present was determined using inductively coupled plasma atomic emission spectrometry on chemically digested portions of samples used in our studies. As a check, one of the crystals (Nd:SFAP) was analyzed independently by Galbraith Laboratories (Knoxville, TN). The results were in agreement with our determinations. The absorption spectra reported in Table I were obtained from samples Nd:SFAP (0.29 at. wt % Nd) and Nd:FAP (0.61 at. wt % Nd). The Nd densities in these crystals are 3×10^{19} and 6×10^{19} ions/cm^3, respectively.

Absorption spectra measured between 2650 and 300 nm were obtained using a Cary model 2390 spectrophotometer equipped with a continuous-flow liquid-helium cryostat that allowed us to observe spectra at any temperature between 4 K and room temperature. Calibration of the instrument was achieved by measurement of standard deuterium emission lines in different orders. Spectral bandwidths were much less than the bandwidths of the majority of absorption peaks observed. The precision in measuring the spectra reported in Table I was generally to within 0.1 nm. Supplemental absorption spectra were recorded using a Perkin–Elmer Lambda 9 spectrophotometer covering the same wavelength range. The instrument was equipped with a liquid-helium conduction dewar. Absorption spectra measured between 4080 and 1920 nm were also obtained at room temperature with a Nicolet 60sx Fourier transform infrared (FTIR) spectrometer.

Using the Cary spectrophotometer, we obtained axial absorption spectra (with the light beam collinear with the c axis of the crystal), and polarized transverse absorption spectra [with the **E** of the light beam perpendicular (σ) and parallel (π) to the c axis of the crystal]. We observed no spectroscopic evidence that would suggest a phase change in either Nd:SFAP or Nd:FAP at temperatures below room temperature.[26] Orientation of the optical axis was determined by placing the crystal between crossed polarizers and observing the characteristic ''Maltese cross'' pattern. We observed no temperature-dependent (hot band) absorption spectra in any of our samples. We conclude that the energy separation between the ground-state Stark level and the first excited Stark level in the $^4I_{9/2}$ manifold is large relative to the thermal energy associated with the temperatures at which our measurements were made.

Site-selective excitation and fluorescence spectra were obtained at 4 and 80 K using a Quantel Nd:YAG laser-pumped dye laser having an output bandwidth of approximately 0.1 cm^{-1}. A 0.85 m double monochromator equipped with a R928 photomultiplier tube (PMT) was used for fluorescence detection and signals were processed using a boxcar averager and gated integrator. Data were collected and stored using a digital oscilloscope. A 0.22 m monochromator and liquid-nitrogen-cooled germanium detector were used to detect fluorescence between 1.0 and 1.5 μm. An Oxford 1204D continuous-flow liquid-helium cryostat allowed us to obtain spectra from samples down to 4 K.

THE OBSERVED SPECTRA

At 4 K numerous absorption bands are observed in the spectra of both crystals. Many bands are relatively broad and have satellite structure. We attribute the spectra to Nd^{3+} ions

TABLE I. Absorption spectra of Nd^{3+} in $Sr_5(PO_4)_3F$ and $Ca_5(PO_4)_3F$.[a]

	Nd:SFAP[c]			Nd:FAP[d]			Nd:FAP[e]			
$^{2s+1}L_J$[b]	λ (Å)[f]	α[g]	E (cm^{-1})[h]	λ (Å)[f]	α[g]	E (cm^{-1})[h]	λ (Å)[f]	α[g]	E (cm^{-1})[h]	P[i]
$^4I_{13/2}$	26 278	0.15	3804	26 190	0.1	3817	25 170	0.02	3972	σ,π
							25 040	0.04	3992	σ,π
							24 620	0.04	4061	σ
							24 560	0.05	4070	σ
							24 370	0.06	4102	σ,π
				23 650	0.6	4227				
	23 390(b)	0.10	4275	23 520	0.4	4251				
				23 220	0.4	4306				
	23 104	0.80	4327				22 980		4350	σ,π
				22 910	0.6	4363	22 930		4360	σ,π
	22 880	0.54	4370	22 780		4389	22 860		4372	σ
	22 542	0.66	4435				22 590		4425	σ,π
	22 476	0.64	4448							
	22 397	1.01	4464							
	21 976	0.48	4549	22 200		4503				
$^4I_{15/2}$	17 510	0.45	5710	17 470		5723	17 375		5754	σ,π
							16 950		5898	σ,π
							16 610		6018	σ
				16 130		6198				
	16 010	0.15	6244				16 034		6235	σ,π
	15 848	0.27	6308	15 850		6307				
				15 740		6352	15 740		6352	σ
	15 662	0.20	6383				15 670		6380	σ,π
	15 549	0.23	6430	15 523		6440				
	15 500	0.23	6450	15 500		6450				
	15 370	0.21	6505	15 210		6573	15 280		6543	σ,π
	15 136	0.19	6605				15 130		6608	σ
	14 880	0.19	6718	14 887		6715				
$^4F_{3/2}$				8870(b)	0.04	11 270				
				8839.8	0.73	11 309				
	8813.0	0.12	11344	8815(b)	0.46	11 341				
	8806.0	1.23	11353							
							8765.0	0.06	11 406	σ,π
							8737(b)	0.02	11 442	σ,π
							8704(b)	0.03	11 486	σ,π
							8664.0	0.08	11 539	σ
				8566.1	0.81	11 671				
	8537.4	1.33	11710							
	8522.2	0.48	11731							
$^4F_{5/2}$	8160.1	0.04	12 251	8120(b)	0.38	12 312				
	8088.3	0.06	12 360	8100.0	1.25	12 342				
	8080.2	0.06	12 373				8085.6	0.20	12 364	σ,π
	8046.4	2.30	12 425				8074(b)	0.13	12 382	σ,π
	8030.0	0.07	12 450				8010.4	0.21	12 480	σ,π
				8003.2	2.03	12 492				
				7977.0	1.52	12 533	7968.2	0.11	12 546	σ
$^2H_{9/2}$				7941.8	2.08	12 588				
	7933.8	1.10	12 601							
							7920.7	0.10	12 622	σ,π
	7905.2	0.43	12 646				7906.1	0.10	12 645	σ
	7881.1	0.79	12 685	7879.0	0.50	12 688				
	7852(b)	0.03	12 730				7840(b)	0.15	12 752	σ,π
	7823.5	0.02	12 779	7835.0	1.13	12 760				
	7797(b)	0.02	12 823	7798.0	0.40	12 820				
							7774.1	0.05	12 860	σ
	7759.9	0.31	12 883				7758.0	0.08	12 886	σ,π
	7721.6	0.21	12 948							
	7706.3	0.12	12 973							
				7506(b)	0.50	13 020				
	7572(b)	0.03	13 202							
$^4F_{7/2}$							7524.0	0.15	13 287	σ,π
				7504.4	2.64	13 326	7505(sh)	0.75	13 320	σ,π

TABLE I. (*Continued*).

	Nd:SFAP[c]			Nd:FAP[d]			Nd:FAP[e]			
$^{2s+1}L_J$[b]	λ (Å)[f]	α[g]	E (cm^{-1})[h]	λ (Å)[f]	α[g]	E (cm^{-1})[h]	λ (Å)[f]	α[g]	E (cm^{-1})[h]	P[i]
	7474.0	0.24	13 376				7487.1	0.40	13 353	σ
	7464.7	1.13	13 393							
				7424.0	1.21	13 460				
				7415.7	1.08	13 481				
$^4S_{3/2}$	7400.1	1.55	13 510	7396.0	0.91	13 517	7397.0	0.25	13 514	σ,π
	7370(b)	0.24	13 565				7395(sh)	0.10	13 519	σ,π
	7364(b)	0.07	13 572							
	7358.2	0.05	13 587							
	7336.3	0.05	13 627	7344	0.97	13 613	7344	0.97	13 613	σ,π
	7332(b)	0.05	13 643							
	7320.9	0.67	13 657							
	7301.4	1.79	13 692							
	7183.7	1.15	13 918	7182(b)	0.56	13 920				
	7172(b)	0.05	13 939							
	7140(b)	0.02	14 000							
$^4F_{9/2}$				6862.2	0.23	14 569				
				6854.0	0.61	14 586				
	6830.7	0.02	14 636							
	6828.2	0.44	14 641				6807.0	0.05	14 687	σ,π
				6780.0	0.14	14 745	6775.5	0.05	14 755	σ,π
							6771.6	0.06	14 763	σ,π
	6715.3	0.11	14 808				6738.1	0.05	14 837	σ,π
				6714.0	0.10	14 890				
	6692.4	0.08	14 939							
				6656(b)	0.07	15 020				
	6667(b)	0.03	15 000	6642.1	0.12	15 052				
	6629(b)	0.02	15 085				6639(sh)	0.06	15 058	σ
	6614.8	0.12	15 113							
$^2H_{11/2}$				6318(b)	0.03	15 823				
	6243.9	0.02	16 011	6264.4	0.08	15 959				
				6222.3	0.10	16 067	6220(b)	0.02	16 067	σ
				6215.0	0.05	16 086	6215(b)	0.01	16 086	σ,π
	6200.3	0.06	16 124	6202(b)	0.04	16 119	6202(b)	0.02	16 119	σ
	6191.1	0.03	16 148	6184.4	0.08	16 165	6198(b)	0.03	16 130	σ,π
	6177.3	0.04	16 185	6160.7	0.10	16 227	6184(b)	0.02	16 165	σ,π
	6159.1	0.05	16 232							
	6132.0	0.06	16 303							
$^4G_{5/2}$				5901.0	1.09	16 942				
				5882.3	4.03	16 995				
	5865.4	1.17	17 044							
$^2G_{7/2}$				5849.8	1.03	17 090	5856.1	0.74	17 071	σ,π
							5815.0	0.73	17 192	σ,π
	5798.0	2.15	17 243	5806.0	3.71	17 219				
	5781.1	2.26	17 293							
				5758.6	3.67	17 361	5763.6	0.36	17 345	σ
	5747.0	1.45	17 396	5741.5	4.00	17 412				
	5726.1	2.27	17 459	5725.0	2.14	17 462				
	5703(b)	0.10	17 540	5704.5	1.56	17 525	5704.3	0.20	17 525	σ,π
	5680.2	1.48	17 600				5680(b)	0.04	17 600	σ,π
							5661(b)	0.03	17 661	σ,π

[a]Spectra obtained at 4 K; total Nd concentration (0.29 at. wt % in SFAP); total Nd concentration (0.56 at. wt % in FAP).
[b]Multiplet manifolds of Nd^{3+} ($4f^3$) split by the crystal field.
[c]Total spectra of Nd^{3+} ions in SFAP.
[d]Spectra of Nd^{3+} ions in fluorescing sites in FAP.
[e]Spectra of Nd^{3+} ions in nonfluorescing sites in FAP.
[f]Wavelength in Å, *b* denotes broad.
[g]Intensity of axial spectra; α is in units of absorbance/cm.
[h]Energy in units of vacuum wave numbers.
[i]Polarization of the transverse spectra.

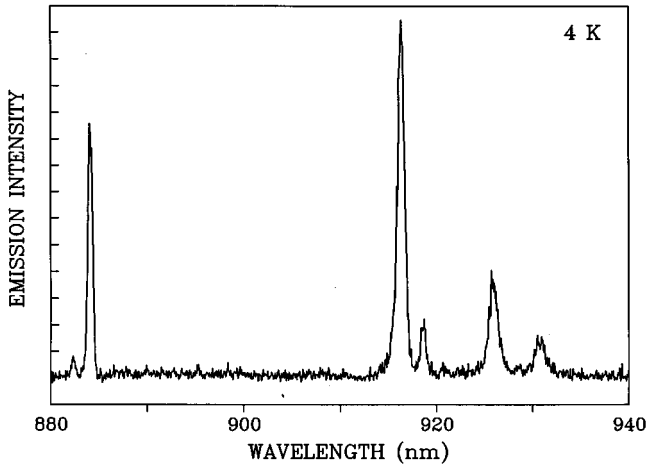

FIG. 1. Emission spectrum at 4 K from the $^4F_{3/2}$ to the $^4I_{9/2}$ ground-state multiplet manifold; excitation of $^4F_{9/2}$ (685 nm) Nd:FAP.

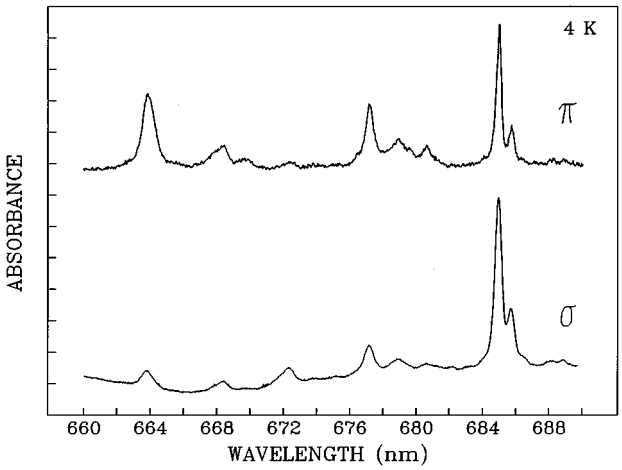

FIG. 3. Polarized absorption spectrum of the $^4F_{9/2}$ multiplet manifold of Nd^{3+} in FAP at 4 K.

residing in different charge-compensated sites. The number of absorption peaks associated with any given multiplet manifold of $Nd^{3+}(4f^3)$ exceeds the expected number of $J+1/2$ transitions from the ground state of the ion in a single site.[27,28] Most of the transitions observed in the spectra taken on crystals of Nd:SFAP (containing 0.29 wt % Nd) and Nd-:FAP (containing 0.61 wt % Nd) appear in both σ and π polarizations in the transverse spectra. In Nd:FAP however, within each multiplet manifold we observe additional moderate to weak absorption peaks primarily in the σ spectrum, along with weak spectra appearing in both polarizations.

Of the two fluorapatite crystals studied, the absorption spectrum of Nd:SFAP is easier to interpret because many fewer satellite peaks are observed within the wavelength range that spans a given multiplet. In fact Table I shows that for each manifold in Nd:SFAP there are usually $J+1/2$ relatively strong peaks accompanied by weaker and usually broader satellite features, suggesting that Nd^{3+} occupation of a single site may dominate the observed spectra. This feature is attributed to the growth conditions of Nd:SFAP, the doping level of Nd^{3+} ions,[8] and the intrinsic lattice properties of Nd:SFAP.

Site-selective excitation and fluorescence methods were used to identify transitions differentiating Nd^{3+} ions in the different sites in Nd:FAP and to confirm that there is a predominant site for Nd^{3+} ions in Nd:SFAP. The fluorescence spectra appearing in Figs. 1 and 2, representing transitions from the $^4F_{3/2}$ manifold to the $^4I_{9/2}$ and $^4I_{11/2}$ manifolds of Nd^{3+} in Nd:FAP, are primarily due to Nd^{3+} ions in only one of several sites. In Fig. 1 selectivity was achieved by narrow band (0.1 cm^{-1}) excitation of the strongest peak (685.4 nm) in the $^4F_{9/2}$ manifold (see Fig. 3 and Table I) followed by nonradiative relaxation to the $^4F_{3/2}$ manifold. In Fig. 2 we selectively excited one of the strong peaks in the $^4G_{5/2}$, $^2G_{7/2}$ grouping at 588 nm. This excitation was followed by nonradiative relaxation to the $^4F_{3/2}$ manifold. Similar experiments involving the same multiplets were carried out on Nd:SFAP where the results gave the expected number of transitions for

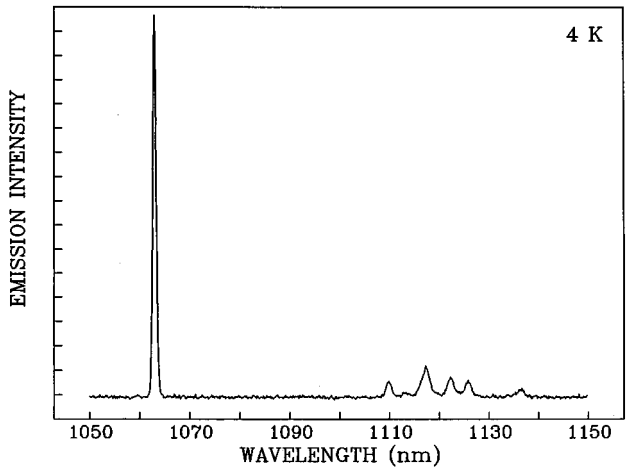

FIG. 2. Emission spectrum at 4 K from the $^4F_{3/2}$ to the $^4I_{11/2}$ multiplet manifold; excitation of $^4G_{5/2}$, $^2G_{7/2}$ (588 nm) Nd:FAP.

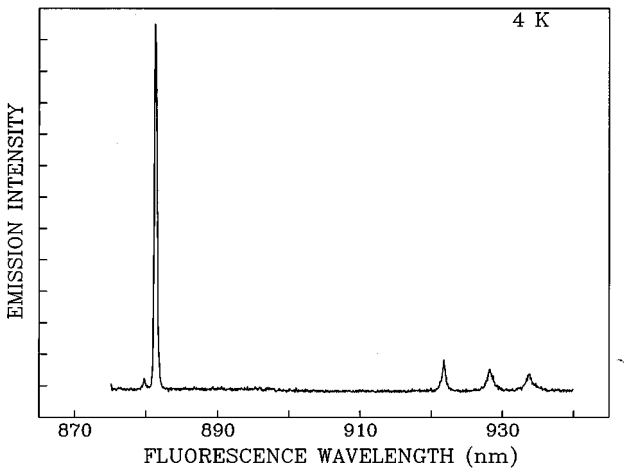

FIG. 4. Emission spectrum at 4 K from the $^4F_{3/2}$ to the $^4I_{9/2}$ ground-state multiplet manifold; excitation of $^4F_{9/2}$ (683 nm) Nd:SFAP.

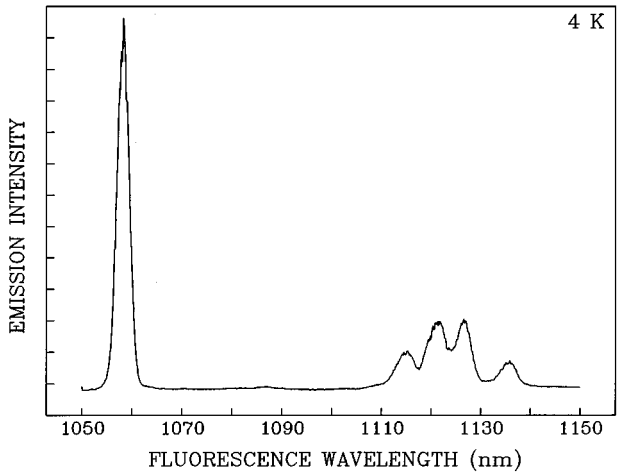

FIG. 5. Emission spectrum at 4 K from the $^4F_{3/2}$ to the $^4I_{11/2}$ multiplet manifold; excitation of $^4G_{5/2}$, $^2G_{7/2}$ (586 nm) Nd:SFAP.

Nd^{3+} in a single site. Figure 4 and 5 present the emission spectra for the corresponding transitions in Nd:SFAP. From Figs. 1 and 2 as well as from Figs. 4 and 5 we can see clearly the large crystal-field splitting of the emitting Nd^{3+} ions. In both Nd:FAP and Nd:SFAP we observe fluorescence only from the $^4F_{3/2}$ manifold. This observation is likely the result of a large crystal-field splitting that greatly mixes states above $^4F_{3/2}$ and the presence of high-energy phonons that in coupling with electronic states can lead to strong nonradiative relaxation processes.[9,24] The crystal-field splittings of the $^4I_{9/2}$ and $^4I_{11/2}$ multiplets obtained from fluorescence measurements are given in Table II for both fluorapatites.

Figure 6 compares the 4 K excitation spectrum obtained by detecting fluorescence at 1063 nm ($^4F_{3/2}\rightarrow{}^4I_{11/2}$, Nd:FAP) with the 4 K axial transmittance spectrum obtained between 500 and 540 nm ($^4G_{9/2}$, $^4G_{7/2}$). The site-selective excitation spectrum consists of five sharp peaks found between 505 and 517 nm (the number expected for $^4G_{9/2}$) and four strong peaks found between 520 and 530 nm (the number expected for $^4G_{7/2}$). Conspicuously absent from the excitation spectrum are peaks associated with Nd^{3+} ions in other sites that are observed in the transmittance spectrum in Fig. 6. When excitation was carried out at wavelengths corresponding to some of these weak peaks in the transmittance spectrum, no fluorescence was observed at, or in the vicinity of 1063 nm.

In Nd:SFAP the absorption spectrum between 500 and 540 nm obtained at 4 K shows a total of nine strong peaks and several very weak broad bands indicating the dominance of a single site, with the $^4G_{9/2}$, $^4G_{7/2}$ multiplets clearly resolved. Further evidence supporting a single fluorescing site in Nd:SFAP can be found by examining the 4 K absorption spectrum of the $^2P_{1/2}$ multiplet. Over 90% of the integrated absorbance is found in a single peak at 431.5 nm with three other peaks at 430.3, 430.9, and 432.5 nm sharing less than 10% in total.

In Fig. 7 we compare the 4 K excitation spectrum produced by detecting fluorescence at 1063 nm ($^4F_{3/2}\rightarrow{}^4I_{11/2}$)

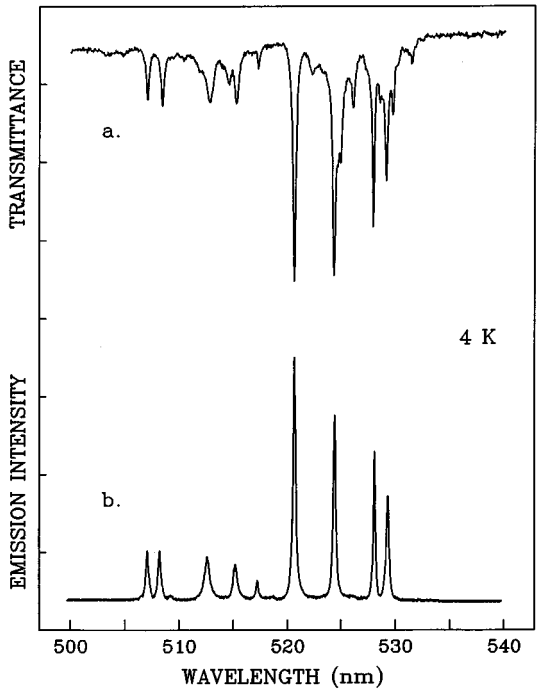

FIG. 6. (a) Transmittance spectrum of the $^4G_{9/2}$, $^4G_{7/2}$ multiplet manifolds at 4 K; (b) site-selective excitation of the $^4G_{9/2}$, $^4G_{7/2}$ multiplets at 4 K Nd:FAP.

in Nd:FAP with the 4 K axial transmittance spectrum between 595 and 565 nm ($^2G_{7/2}$, $^4G_{5/2}$). The site-selective excitation spectrum is sharp, with three peaks (one possibly with a shoulder) found between 570 and 578 nm (the $^2G_{7/2}$

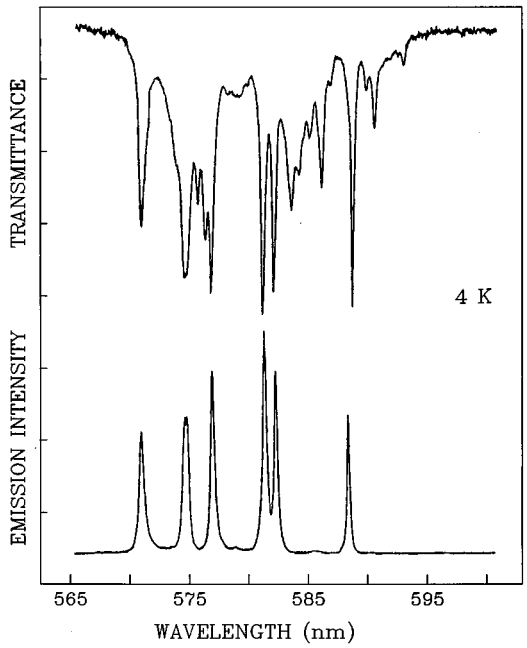

FIG. 7. (a) Transmittance spectrum of the $^2G_{7/2}$, $^4G_{5/2}$ multiplet manifolds at 4 K; (b) site-selective excitation of the $^2G_{7/2}$, $^4G_{5/2}$ multiplets at 4 K Nd:FAP.

TABLE II. Emission from $^4F_{3/2}$ to $^4I_{9/2}$ and $^4I_{11/2}$ at 4 K.

Nd:SFAP				Nd:FAP			
λ (Å)[a]	E (cm^{-1})[b]	I[c]	ΔE (cm^{-1})[d]	λ (Å)[a]	E (cm^{-1})[b]	I[c]	ΔE (cm^{-1})[d]
8797.0	11 364	vw	⋯	8823.2	11 331	vw	⋯
8812.0	11 345	vss	0	8840.4	11 309	vss	0
9217.1	10 847	m	498	9163.2	10 910	vs	399
				9186.2	10 883	w	
9282.1	10 771	m	574	9259.3	10 797	m	512
9337.0	10 707	m	638	9306.7	10 742	w	567
9444	10 585	m	760	9429	10 602	w	707
10 583	9447	vs	1899	10 628	9407	vss	1902
11 100(sh)	9007	w	2340	11 099	9007	w	2302
11 148	8968	w	2378	11 140	8974	vw	2335
				11 174	8947	vw	
11 212	8917	m	2429	11 229	8903	w	2406
11 264	8875	m	2470	11 258	8880	w	2429
11 355	8804	w	2541	11 367	8795	w	2514

[a]Wavelength in Å.
[b]Energy of transition in units of vacuum wave numbers.
[c]Relative intensity within a manifold: vw (very weak); w (weak); m (moderate); s (strong); vs (very strong); vss (strongest).
[d]Splitting of the multiplet manifold in cm^{-1}; energy of the Stark level.

multiplet), and three peaks observed between 580 and 590 nm (the $^4G_{5/2}$ multiplet). Clearly the simplicity and spectral resolution of the exciting laser, relative to the transmittance obtained from the Cary spectrophotometer, point to the advantage of using narrow-band laser excitation to differentiate between ions in different sites. The corresponding absorption spectrum at 4 K for Nd:SFAP (Table I) includes six very strong lines, a weak/broad band (570.6 nm) and very weak shoulders around the base of most of the strong lines that were too difficult to measure systematically. The simplicity of the spectrum supports the notion that Nd^{3+} ions are found predominantly in a single site in Nd:SFAP.

Returning to Fig. 7, we tried excitation at wavelengths corresponding to absorption by Nd^{3+} ions in other sites in Nd:FAP, but failed to generate fluorescence. This suggests that perhaps while Nd^{3+} ions in numerous sites may absorb energy, only those in one of the sites fluoresce. Those that reside in the remaining so-called ''dead'' sites lose their energy nonradiatively; energy transfer to a different fluorescing center is not evident.

Laser excitation of Nd:FAP was also carried out while total fluorescence from the $^4F_{3/2}$ manifold was measured nondispersively. This was accomplished by placing a high-pass optical filter in front of the germanium detector to allow detection of wavelengths greater than 800 nm. This permitted the simultaneous detection of all fluorescence associated with transitions between the $^4F_{3/2}$ manifold, and the $^4I_{9/2}$ and $^4I_{11/2}$ manifold for Nd^{3+} ions in all sites. These experiments indicate that the fluorescence originated primarily from a single site, identified as the fluorescing site.

DISCUSSION AND CALCULATIONS

The spectra reported in Table I were obtained from Nd^{3+}-doped fluorapatite crystals which have a hexagonal structure that belongs to the $P6_3/m$ (# 176) space group with two molecules per unit cell.[22] The divalent metal ions (Sr, Ca) occupy two sites, M(I) in the $4f$ site with C_3 symmetry and M(II) in the $6h$ site with C_s symmetry. The ratio of metal ions in these two sites is 60 to 40. Surrounding the M(I) site are six nearest-neighbor oxygen ions that form a distorted triangular prism. The M(II) sites sit at the corners of equilateral triangles with the F^- ion in the center. Substitution of trivalent neodymium for a divalent cation was achieved by passive charge compensation during crystal growth.[1]

Recently, Morrison[27] completed a point charge analysis of symmetry-preserving charge compensation and vacancies in the fluorapatites doped with Nd^{3+} ions. Our approach in the present study has been to calculate the crystal-field splitting of the energy levels of Nd:SFAP and Nd:FAP by considering the symmetry of the site[27,28] and the subsequent data sets as the primary guide to the phenomenological set of crystal-field parameters B_{nm} obtained from the analysis. To interpret the splitting of the levels in the fluorescing sites, we used as a starting set of B_{nm} the values reported by Peale *et al.*[5] for Nd:SVAP. Our calculations were based on C_s symmetry, the same symmetry used in Ref. 5.

The total Hamiltonian for the Nd^{3+} ion includes terms representing the free-ion and the crystal electric-field interactions. The Racah and spin-orbit parameters entering into the free-ion Hamiltonian were derived from an analysis of the aqueous solution spectra.[30] The appropriate values as well as the details of the computation are given elsewhere.[30–34] The crystal-field Hamiltonian is of the form

$$H_{\mathrm{CEF}} = \sum_{n}\sum_{\mathrm{even}}\sum_{m=-n}^{n} B_{nm}^{*}\sum_{i=1}^{N} C_{nm}(i), \tag{1}$$

where the B_{nm} are the crystal-field parameters and the expressions C_{nm} are given as

TABLE III. Crystal-field splitting: Nd^{3+} ions in C_s sites

$^{2S+1}L_J$[a]	No.[b]	E (cm^{-1})[c] (expt.)	E (cm^{-1})[d] (calc.)	Free-ion percent mixture
$^4I_{9/2}$	1	0	6.0	$97.7\ ^4I_{9/2}+2.12\ ^4I_{11/2}+0.12\ ^4I_{13/2}$
545	1	0	−0.4	$98.1\ ^4I_{9/2}+1.72\ ^4I_{11/2}+0.10\ ^4I_{13/2}$
(482)	2	498	486	$98.9\ ^4I_{9/2}+0.76\ ^4I_{11/2}+0.19\ ^4G_{5/2}$
	2	399	387	$98.7\ ^4I_{9/2}+1.00\ ^4I_{11/2}+0.15\ ^4G_{5/2}$
	3	574	566	$99.2\ ^4I_{9/2}+0.55\ ^4I_{11/2}+0.11\ ^4G_{5/2}$
	3	512	512	$99.5\ ^4I_{9/2}+0.32\ ^4I_{11/2}+0.10\ ^4G_{5/2}$
	4	638	647	$98.2\ ^4I_{9/2}+1.64\ ^4I_{11/2}+0.08\ ^4I_{13/2}$
	4	567	575	$99.0\ ^4I_{9/2}+0.84\ ^4I_{11/2}+0.10\ ^4G_{5/2}$
	5	760	764	$99.0\ ^4I_{9/2}+0.73\ ^4I_{11/2}+0.13\ ^4G_{5/2}$
	5	707	712	$98.8\ ^4I_{9/2}+0.96\ ^4I_{11/2}+0.11\ ^4G_{5/2}$
$^4I_{11/2}$	6	1899	1907	$95.8\ ^4I_{11/2}+2.17\ ^4I_{13/2}+1.88\ ^4I_{9/2}$
2361	6	1902	1911	$97.0\ ^4I_{11/2}+1.84\ ^4I_{13/2}+1.04\ ^4I_{9/2}$
(2332)	7	2340	2339	$97.4\ ^4I_{11/2}+1.62\ ^4I_{9/2}+0.87\ ^4I_{13/2}$
	7	2302	2307	$98.1\ ^4I_{11/2}+1.15\ ^4I_{9/2}+0.64\ ^4I_{13/2}$
	8	2378	2368	$98.3\ ^4I_{11/2}+0.77\ ^4I_{9/2}+0.68\ ^4I_{13/2}$
	8	2335	2327	$98.2\ ^4I_{11/2}+0.89\ ^4I_{9/2}+0.71\ ^4I_{13/2}$
	9	2429	2418	$98.9\ ^4I_{11/2}+0.54\ ^4I_{13/2}+0.43\ ^4I_{9/2}$
	9	2406	2393	$99.0\ ^4I_{11/2}+0.58\ ^4I_{9/2}+0.32\ ^4I_{13/2}$
	10	2470	2471	$98.6\ ^4I_{11/2}+0.71\ ^4I_{9/2}+0.50\ ^4I_{13/2}$
	10	2429	2431	$98.5\ ^4I_{11/2}+0.80\ ^4I_{9/2}+0.56\ ^4I_{13/2}$
	11	2541	2546	$98.5\ ^4I_{11/2}+0.80\ ^4I_{13/2}+0.47\ ^4I_{9/2}$
	11	2514	2521	$98.4\ ^4I_{11/2}+0.93\ ^4I_{13/2}+0.45\ ^4I_{9/2}$
$^4I_{13/2}$	12	3804	3815	$96.6\ ^4I_{13/2}+1.69\ ^4I_{15/2}+1.54\ ^4I_{11/2}$
4323	12	3817	3799	$97.6\ ^4I_{13/2}+1.38\ ^4I_{15/2}+0.95\ ^4I_{11/2}$
(4271)	13	4275	4275	$96.4\ ^4I_{13/2}+2.25\ ^4I_{11/2}+1.20\ ^4I_{15/2}$
	13	4227	4220	$97.3\ ^4I_{13/2}+1.80\ ^4I_{11/2}+0.78\ ^4I_{15/2}$
	14	4327	4328	$99.1\ ^4I_{13/2}+0.45\ ^4I_{15/2}+0.19\ ^4I_{11/2}$
	14	4251	4258	$98.9\ ^4I_{13/2}+0.59\ ^4I_{15/2}+0.40\ ^4I_{11/2}$
	15	4370	4370	$99.1\ ^4I_{13/2}+0.55\ ^4I_{15/2}+0.27\ ^4I_{11/2}$
	15	4306	4321	$99.3\ ^4I_{13/2}+0.34\ ^4I_{15/2}+0.25\ ^4I_{11/2}$
	16	⋯	4419	$98.5\ ^4I_{13/2}+0.75\ ^4I_{11/2}+0.63\ ^4I_{15/2}$
	16	4363	4357	$98.4\ ^4I_{13/2}+0.89\ ^4I_{11/2}+0.57\ ^4I_{15/2}$
	17	4464	4455	$99.0\ ^4I_{13/2}+0.47\ ^4I_{15/2}+0.39\ ^4I_{11/2}$
	17	4389	4395	$99.0\ ^4I_{13/2}+0.50\ ^4I_{15/2}+0.36\ ^4I_{11/2}$
	18	4549	4549	$98.7\ ^4I_{13/2}+0.75\ ^4I_{15/2}+0.28\ ^4I_{11/2}$
	18	4503	4505	$98.7\ ^4I_{13/2}+0.84\ ^4I_{15/2}+0.32\ ^4I_{11/2}$
$^4I_{15/2}$	19	5710	5701	$98.2\ ^4I_{15/2}+1.66\ ^4I_{13/2}+0.09\ ^4I_{11/2}$
6362	19	5723	5733	$98.9\ ^4I_{15/2}+0.99\ ^4I_{13/2}+0.06\ ^4I_{11/2}$
(6361)	20	6244	6250	$98.4\ ^4I_{15/2}+1.38\ ^4I_{13/2}+0.08\ ^4F_{9/2}$
	20	6198	6203	$98.6\ ^4I_{15/2}+1.15\ ^4I_{13/2}+0.06\ ^4F_{9/2}$
	21	6308	6312	$99.3\ ^4I_{15/2}+0.46\ ^4I_{13/2}+0.07\ ^4F_{9/2}$
	21	6307	6298	$99.2\ ^4I_{15/2}+0.66\ ^4I_{13/2}+0.05\ ^4F_{7/2}$
	22	6383	6387	$99.2\ ^4I_{15/2}+0.57\ ^4I_{13/2}+0.07\ ^4I_{11/2}$
	22	6352	6357	$99.4\ ^4I_{15/2}+0.48\ ^4I_{13/2}+0.04\ ^4I_{11/2}$
	23	6450	6453	$99.0\ ^4I_{15/2}+0.79\ ^4I_{13/2}+0.05\ ^4F_{9/2}$
	23	6440	6433	$99.6\ ^4I_{15/2}+0.32\ ^4I_{13/2}+0.04\ ^4I_{11/2}$
	24	6505	6510	$99.5\ ^4I_{15/2}+0.36\ ^4I_{13/2}+0.03\ ^4I_{11/2}$
	24	6450	6457	$99.0\ ^4I_{15/2}+0.74\ ^4I_{13/2}+0.07\ ^4F_{9/2}$
	25	6605	6602	$99.6\ ^4I_{15/2}+0.32\ ^4I_{13/2}+0.03\ ^4F_{7/2}$
	25	6573	6569	$99.6\ ^4I_{15/2}+0.28\ ^4I_{13/2}+0.04\ ^4F_{7/2}$
	26	6718	6710	$99.5\ ^4I_{15/2}+0.26\ ^4I_{13/2}+0.07\ ^4F_{9/2}$
	26	6715	6708	$99.5\ ^4I_{15/2}+0.28\ ^4I_{13/2}+0.05\ ^4F_{7/2}$
$^4F_{3/2}$	27	11 353	11 358	$93.7\ ^4F_{3/2}+4.61\ ^4F_{5/2}+0.56\ ^4F_{7/2}$
11 666	27	11 309	11 322	$94.1\ ^4F_{3/2}+4.42\ ^4F_{5/2}+0.50\ ^4G_{5/2}$
(11 614)	28	11 710	11 706	$91.8\ ^4F_{3/2}+5.00\ ^4F_{5/2}+1.40\ ^5G_{5/2}$
	28	11 671	11 658	$92.1\ ^4F_{3/2}+5.22\ ^4F_{5/2}+1.25\ ^4G_{5/2}$
$^4F_{5/2}$	29	12 425	12 431	$82.1\ ^4F_{5/2}+7.48\ ^2H_{9/2}+5.37\ ^4F_{7/2}$
12 697	29	12 342	12 345	$78.1\ ^4F_{5/2}+12.9\ ^2H_{9/2}+4.55\ ^4F_{7/2}$
(12 593)	30	12 601	12 601	$52.7\ ^4F_{5/2}+41.7\ ^2H_{9/2}+2.53\ ^4F_{3/2}$
	30	12 492	12 475	$76.7\ ^2H_{9/2}+20.7\ ^4F_{5/2}+1.16\ ^4F_{3/2}$

TABLE III. (*Continued*.)

$^{2S+1}L_J$[a]	No.[b]	E (cm^{-1})[c] (expt.)	E (cm^{-1})[d] (calc.)	Free-ion percent mixture
$^2H_{9/2}$	31	12 664	12 685	61.1 $^2H_{9/2}$+35.2 $^4F_{5/2}$+1.67 $^4F_{3/2}$
12 912	31	12 533	12 532	56.1 $^4F_{5/2}$+38.6 $^2H_{9/2}$+2.75 $^4F_{3/2}$
(12 375)	32	⋯	12 736	56.4 $^4F_{5/2}$+40.1 $^2H_{9/2}$+1.08 $^4F_{3/2}$
	32	12 588	12 589	50.4 $^2H_{9/2}$+46.4 $^4F_{5/2}$+1.21 $^4F_{3/2}$
	33	⋯	12 820	76.1 $^2H_{9/2}$+20.3 $^4F_{5/2}$+1.48 $^4F_{3/2}$
	33	12 688	12 676	63.4 $^2H_{9/2}$+32.9 $^4F_{5/2}$+1.90 $^4F_{3/2}$
	34	12 948	12 951	88.9 $^2H_{9/2}$+9.07 $^4F_{5/2}$+1.13 $^4F_{7/2}$
	34	12 760	12 772	85.1 $^2H_{9/2}$+13.0 $^4F_{5/2}$+1.08 $^4F_{7/2}$
	35	12 973	12 984	81.1 $^2H_{9/2}$+16.7 $^4F_{5/2}$+1.63 $^4F_{7/2}$
	35	12 820	12 829	70.3 $^2H_{9/2}$+27.5 $^4F_{5/2}$+1.51 $^4F_{7/2}$
	36	⋯	13 215	96.5 $^2H_{9/2}$+2.04 $^4F_{5/2}$+0.63 $^4F_{9/2}$
	36	13 020	13 024	96.9 $^2H_{9/2}$+1.81 $^4F_{5/2}$+0.54 $^4F_{9/2}$
$^4S_{3/2}$	37	13 393	13 396	89.8 $^4F_{7/2}$+3.82 $^4F_{5/2}$+3.52 $^4F_{9/2}$
13 554	37	13 322	13 327	92.3 $^4F_{7/2}$+2.87 $^4F_{9/2}$+2.54 $^4F_{5/2}$
(13 498)	38	13 510	13 513	93.5 $^4S_{3/2}$+5.07 $^4F_{7/2}$+0.49 $^4G_{5/2}$
	38	13 460	13 461	80.4 $^4S_{3/2}$+17.3 $^4F_{7/2}$+0.83 $^4F_{5/2}$
$^4F_{7/2}$	39	13 565	13 561	61.0 $^4F_{7/2}$+32.8 $^4S_{3/2}$+2.76 $^4F_{5/2}$
13 676	39	13 481	13 490	73.3 $^4F_{7/2}$+20.1 $^4S_{3/2}$+3.29 $^4F_{5/2}$
(13 597)	40	13 572	13 574	70.4 $^4S_{3/2}$+26.2 $^4F_{7/2}$+1.55 $^4F_{5/2}$
	40	13 517	13 515	97.1 $^4S_{3/2}$+2.12 $^4F_{7/2}$+0.18 $^4F_{9/2}$
	41	13 692	13 692	93.4 $^4F_{7/2}$+2.76 $^4F_{9/2}$+1.21 $^4F_{5/2}$
	41	13 613	13 611	94.4 $^4F_{7/2}$+2.24 $^4F_{9/2}$+1.33 $^4F_{5/2}$
	42	⋯	13 998	95.1 $^4F_{7/2}$+1.58 $^2H_{9/2}$+1.10 $^2G_{7/2}$
	42	13 920	13 910	95.7 $^4F_{7/2}$+1.21 $^4F_{9/2}$+1.20 $^2H_{9/2}$
$^4F_{9/2}$	43	14 641	14 627	95.9 $^4F_{9/2}$+1.96 $^4F_{7/2}$+0.89 $^4F_{5/2}$
14 901	43	14 586	14 584	96.9 $^4F_{9/2}$+1.42 $^4F_{7/2}$+0.67 $^4F_{5/2}$
(14 845)	44	14 808	14 813	94.3 $^4F_{9/2}$+4.42 $^4F_{7/2}$+0.54 $^2H_{11/2}$
	44	14 745	14 742	95.3 $^4F_{9/2}$+3.66 $^4F_{7/2}$+0.47 $^2H_{11/2}$
	45	14 939	14 946	94.3 $^4F_{9/2}$+3.20 $^4F_{7/2}$+1.90 $^2H_{11/2}$
	45	14 890	14 893	94.9 $^4F_{9/2}$+2.94 $^4F_{7/2}$+1.58 $^2H_{11/2}$
	46	⋯	15 083	95.5 $^4F_{9/2}$+2.62 $^2H_{11/2}$+1.09 $^2G_{7/2}$
	46	15 020	15 020	95.8 $^4F_{9/2}$+2.33 $^2H_{11/2}$+0.96 $^2G_{7/2}$
	47	15 113	15 117	94.5 $^4F_{9/2}$+4.59 $^2H_{11/2}$+0.38 $^2H_{9/2}$
	47	15 052	15 054	95.1 $^4F_{9/2}$+4.06 $^2H_{11/2}$+0.36 $^2H_{9/2}$
$^2H_{11/2}$	48	⋯	16 086	98.4 $^2H_{11/2}$+0.94 $^2G_{7/2}$+0.20 $^4F_{9/2}$
	48	16 067	16 069	98.7 $^2H_{11/2}$+0.60 $^2G_{7/2}$+0.21 $^4F_{9/2}$
16 152	49	16 124	16 119	98.5 $^2H_{11/2}$+0.50 $^4F_{9/2}$+0.50 $^2G_{7/2}$
(16 128)	49	16 086	16 093	98.7 $^2H_{11/2}$+0.52 $^4F_{9/2}$+0.36 $^2G_{7/2}$
	50	16 148	16 145	97.7 $^2H_{11/2}$+1.17 $^4F_{9/2}$+0.51 $^2G_{7/2}$
	50	16 119	16 123	98.2 $^2H_{11/2}$+1.02 $^4F_{9/2}$+0.33 $^2G_{7/2}$
	51	16 185	16 189	96.8 $^2H_{11/2}$+1.46 $^2G_{7/2}$+1.25 $^4F_{9/2}$
	51	16 165	16 169	96.9 $^2H_{11/2}$+1.41 $^4F_{9/2}$+1.14 $^2G_{7/2}$
	52	16 232	16 243	98.1 $^2H_{11/2}$+1.05 $^4F_{9/2}$+0.57 $^2G_{7/2}$
	52	16 227	16 210	98.6 $^2H_{11/2}$+0.68 $^4F_{9/2}$+0.42 $^2G_{7/2}$
	53	16 303	16 300	93.4 $^2H_{11/2}$+5.03 $^4F_{9/2}$+0.73 $^2H_{9/2}$
	53	⋯	16 261	94.5 $^2H_{11/2}$+4.37 $^4F_{9/2}$+0.58 $^2H_{9/2}$
$^4G_{5/2}$	54	17 044	17 041	56.4 $^4G_{5/2}$+41.0 $^2G_{7/2}$+0.93 $^4F_{3/2}$
17 164	54	16 995	16 987	91.9 $^4G_{5/2}$+5.03 $^2G_{7/2}$+1.93 $^4F_{3/2}$
(17 041)	55	⋯	17 137	67.5 $^4G_{5/2}$+29.3 $^2G_{7/2}$+1.51 $^4F_{3/2}$
	55	17 090	17 087	78.1 $^4G_{5/2}$+20.1 $^2G_{7/2}$+0.56 $^4F_{3/2}$
	56	17 243	17 239	75.1 $^2G_{7/2}$+22.6 $^4G_{5/2}$+0.81 $^2H_{11/2}$
	56	17 219	17 234	60.2 $^4G_{5/2}$+37.1 $^2G_{7/2}$+1.11 $^4F_{5/2}$

TABLE III. (*Continued*.)

$^{2S+1}L_J$[a]	No.[b]	E (cm^{-1})[c] (expt.)	E (cm^{-1})[d] (calc.)	Free-ion percent mixture
$^2G_{7/2}$	57	17 293	17 296	$90.7\ ^2G_{7/2}+6.87\ ^4G_{5/2}+1.24\ ^4F_{5/2}$
17 217	57	17 361	17 358	$74.2\ ^2G_{7/2}+24.1\ ^4G_{5/2}+1.16\ ^4F_{5/2}$
(17 323)	58	17 396	17 392	$63.7\ ^2G_{7/2}+33.4\ ^4G_{5/2}+0.97\ ^2H_{11/2}$
	58	17 412	17 404	$92.9\ ^2G_{7/2}+5.35\ ^4G_{5/2}+0.69\ ^2H_{11/2}$
	59	17 459	17 462	$64.4\ ^2G_{7/2}+32.4\ ^4G_{5/2}+0.98\ ^4F_{9/2}$
	59	17 462	17 468	$72.7\ ^2G_{7/2}+26.1\ ^4G_{5/2}+0.30\ ^2H_{11/2}$
	60	17 540	17 540	$73.7\ ^4G_{5/2}+24.4\ ^2G_{7/2}+0.58\ ^4F_{7/2}$
	60	17 525	17 527	$89.2\ ^2G_{7/2}+7.64\ ^4G_{5/2}+1.02\ ^4F_{7/2}$

[a]Multiplet manifold of Nd^{3+} ($4f^3$); the centroid is given in cm^{-1}; the number without parentheses is the energy for Nd:SFAP; the number with parentheses is the energy for Nd:FAP.
[b]First number in the pair represents the splitting for Nd:SFAP; the second number represents the splitting for Nd:FAP in the fluorescing site.
[c]Experimental data from Tables I and II.
[d]Calculated splitting based on B_{nm} parameters given in Table IV.

$$C_{nm}(i)=\left(\frac{4\pi}{(2n+1)}\right)^{1/2} Y_{nm}(\theta_i,\phi_i), \tag{2}$$

with

$$C_{n-m}=(-1)^m C^*_{nm}, \tag{3}$$

and the Y_{nm} are the usual spherical harmonics. In C_s symmetry, the values of m are restricted by $n+m=0,\pm2,\pm4$, with $|m|\leqslant n$ and $n=2$, 4, and 6. The crystal-field splitting is predominately determined by the n even B_{nm} parameters. For C_s symmetry this number is restricted to 15, but with a simple rotation about the principal axis (c axis), B_{22} can be made real and positive and the number of parameters is then reduced to 14.

In Table III we present the results for the lowest 13 multiplet manifolds of Nd^{3+} ions in sites that fluoresce in Nd:SFAP and Nd:FAP. Because of the size of the splittings, the free-ion percent mixture is also included. Multiplet manifolds $^4F_{5/2}$, $^2H_{9/2}$, and $^4F_{7/2}$, $^4S_{3/2}$ are highly mixed making their $^{2S+1}L_J$ manifold assignments problematic for individual Stark levels. We made repeated attempts to improve our analysis by using B_{nm} parameters obtained from lattice-sum calculations by Morrison[27] based on different charge-compensated models for Nd^{3+} ions in M(II) sites. These efforts did not lead to any success. The final set of phenomenological B_{nm} parameters is compared in Table IV with the set reported for Nd:SVAP (our initial starting set). The similarity in sign and magnitude among the dominant terms, including parameters B_{20}, B_{22}, and B_{40}, suggest a common symmetry site is involved in all three crystals. Variation among smaller parameters is due to our inclusion of numerous excited multiplet manifolds that are so highly mixed (see Table III) that relatively small changes in the crystal-field environment cause large changes in the J mixing among these manifolds. Peale *et al.*[5] restricted their analysis to the splitting of the ^4I_J and $^4F_{3/2}$ manifolds alone.

TABLE IV. Final set of B_{nm} parameters for Nd^{3+} ions in fluorescing sites.

B_{nm} parameter	SFAP[a] (cm^{-1})	FAP[b] (cm^{-1})	SVAP[c] (cm^{-1})
B_{20}	2647	2528	2452
B_{22}	533	520	410
B_{40}	2075	1896	2219
Re B_{42}	−138	−278	320
$I_m B_{42}$	883	439	57.6
Re B_{44}	136	53.4	−148
$I_m B_{44}$	223	444	−186
B_{60}	592	483	435
Re B_{62}	173	289	−81.3
$I_m B_{62}$	514	427	253
Re B_{64}	−13.6	−170	−255
$I_m B_{64}$	−514	−473	122
Re B_{66}	−362	−407	266
$I_m B_{66}$	−16.9	−131	395

[a]rms derivation: 7 cm^{-1}, 52 levels (this work).
[b]rms derivation: 8 cm^{-1}, 59 levels (this work).
[c]rms derivation: 6 cm^{-1}, 28 levels (Ref. 5).

We also carried out crystal-field splitting calculations for Nd^{3+} ions occupying C_3 sites in Nd:FAP. In this case we found that one of Morrison's lattice-sum calculations provided us with a reasonable starting set of B_{nm} parameters.[27,35,36] This model involves the substitution of Nd^{3+} ions into M(I) sites, assuming that the charge compensation is sufficiently remote so that C_3 symmetry is preserved. Maksimova and Sobol[15,16] also describe a charge-compensation model of this type. Since we observe no fluorescence for this site on which to base our assignments, we chose the symmetry of the ground-state Stark level to be $\Gamma_{4,5}$ as predicted using the Morrison parameters.[27] This choice is also consistent with the observed polarized absorption spectra using C_3 symmetry selection rules.[28] The results of these calculations are given in Table V for multiplet manifolds above $^4I_{11/2}$ where the experimental energy levels can be drawn from Table I since no emission to the $^4I_{9/2}$ and $^4I_{11/2}$ manifolds was observed. Again, the most difficult Stark levels to identify are those with a high degree of J mixing. The $^4F_{5/2}$, $^2H_{9/2}$ manifolds and the $^4F_{7/2}$, $^4S_{3/2}$ manifolds represent the most difficult manifolds to analyze.

In Table VI we see that relatively small changes in the

TABLE V. Crystal-field splitting: Nd^{3+} ions in C_3 sites in Nd:FAP.

$^{2S+1}L_J$[a]	Level	E (cm^{-1})[b] (expt.)	Γ_n[c] (expt.)	E (cm^{-1})[d] (calc.)	Γ_n[d] (calc.)	Free-ion percent mixture
$^4I_{9/2}$	1	0		0.2	4,5	98.3 $^4I_{9/2}$+1.51 $^4I_{11/2}$+0.12 $^4I_{13/2}$
(427)	2	⋯		270	6	97.5 $^4I_{9/2}$+2.07 $^4I_{11/2}$+0.32 $^4I_{13/2}$
	3	⋯		356	4,5	97.4 $^4I_{9/2}$+2.40 $^4I_{11/2}$+0.06 $^4G_{5/2}$
	4	⋯		547	4,5	98.7 $^4I_{9/2}$+0.90 $^4I_{11/2}$+0.16 $^4I_{13/2}$
	5	⋯		675	6	97.3 $^4I_{9/2}$+2.45 $^4I_{11/2}$+0.09 $^4I_{13/2}$
$^4I_{11/2}$	6	⋯		2043	6	96.4 $^4I_{11/2}$+2.20 $^4I_{9/2}$+1.29 $^4I_{13/2}$
(2261)	7	⋯		2133	4,5	96.8 $^4I_{11/2}$+2.54 $^4I_{9/2}$+0.29 $^4I_{13/2}$
	8	⋯		2147	4,5	95.2 $^4I_{11/2}$+2.38 $^4I_{9/2}$+2.25 $^4I_{13/2}$
	9	⋯		2348	4,5	96.8 $^4I_{11/2}$+1.72 $^4I_{9/2}$+1.31 $^4I_{13/2}$
	10	⋯		2387	4,5	98.9 $^4I_{11/2}$+0.40 $^4I_{9/2}$+0.33 $^4I_{13/2}$
	11	⋯		2395	6	96.6 $^4I_{11/2}$+2.32 $^4I_{9/2}$+0.91 $^4I_{13/2}$
$^4I_{13/2}$	12	3992	4,5	3989	4,5	96.9 $^4I_{13/2}$+2.01 $^4I_{11/2}$+1.02 $^4I_{15/2}$
(4249)	13	4061	6	4064	6	96.2 $^4I_{13/2}$+1.95 $^4I_{15/2}$+1.49 $^4I_{11/2}$
	14	4102	4,5	4099	4,5	96.4 $^4I_{13/2}$+3.02 $^4I_{15/2}$+0.42 $^4I_{11/2}$
	15	4350	4,5	4350	4,5	97.9 $^4I_{13/2}$+1.02 $^4I_{11/2}$+0.74 $^4I_{15/2}$
	16	4360	4,5	4365	4,5	96.3 $^4I_{13/2}$+1.85 $^4I_{15/2}$+1.61 $^4I_{15/2}$
	17	4372	6	4375	6	97.9 $^4I_{13/2}$+1.07 $^4I_{15/2}$+0.67 $^4I_{11/2}$
	18	4425	4,5	4417	4,5	98.1 $^4I_{13/2}$+1.00 $^4I_{11/2}$+0.74 $^4I_{15/2}$
$^4I_{15/2}$	19	5754	4,5	5752	4,5	96.9 $^4I_{15/2}$+2.91 $^4I_{13/2}$+0.05 $^4F_{9/2}$
(6211)	20	5898	4,5	5899	4,5	98.5 $^4I_{15/2}$+1.18 $^4I_{13/2}$+0.22 $^4I_{11/2}$
	21	6018	6	6014	6	98.9 $^4I_{15/2}$+0.91 $^4I_{13/2}$+0.05 $^4F_{9/2}$
	22	6235	4,5	6236	4,5	98.5 $^4I_{15/2}$+1.17 $^4I_{13/2}$+0.11 $^4I_{11/2}$
	23	6352	6	6358	6	99.2 $^4I_{15/2}$+0.42 $^4I_{13/2}$+0.11$^4F_{9/2}$
	24	6380	4,5	6376	4,5	98.8 $^4I_{15/2}$+0.74 $^4I_{13/2}$+0.14 $^4F_{9/2}$
	25	6543	4,5	6547	4,5	98.5 $^4I_{15/2}$+1.11 $^4I_{13/2}$+0.10 $^4F_{9/2}$
	26	6608	6	6605	6	98.2 $^4I_{15/2}$+1.64 $^4I_{13/2}$+0.07 $^4I_{11/2}$
$^4F_{3/2}$	27	11 406	4,5	11 399	4,5	97.5 $^4F_{3/2}$+0.88 $^4F_{3/2}$+0.57 $^2H_{9/2}$
(11520)	28	11 539	6	11 543	6	93.9 $^4F_{3/2}$+3.88 $^4F_{5/2}$+1.17 $^4F_{7/2}$
$^4F_{5/2}$	29	12 364	4,5	12 361	4,5	85.8 $^4F_{5/2}$+11.7 $^2H_{9/2}$+1.19 $^4F_{7/2}$
(12 536)	30	12 480	4,5	12 483	4,5	65.2 $^4F_{5/2}$+28.5 $^2H_{9/2}$+4.92 $^4F_{7/2}$
	31	12 546	6	12 546	6	86.3 $^2H_{9/2}$+11.1 $^4F_{5/2}$+1.12 $^4F_{3/2}$
$^2H_{9/2}$	32	12 622	4,5	12 626	4,5	70.5 $^2H_{9/2}$+28.0 $^4F_{5/2}$+0.74 $^4F_{7/2}$
	33	12 645	6	12 644	6	83.0 $^4F_{5/2}$+12.6 $^2H_{9/2}$+3.58 $^4F_{3/2}$
(12 726)	34	12 752	4,5	12 759	4,5	87.4 $^2H_{9/2}$+10.5 $^4F_{5/2}$+1.42 $^4F_{7/2}$
	35	12 860	6	12 854	6	98.7 $^2H_{9/2}$+0.69 $^4F_{5/2}$+0.23 $^4F_{9/2}$
	36	12 886	4,5	12 891	4,5	97.8 $^2H_{9/2}$+1.34 $^4F_{7/2}$+0.33 $^4F_{5/2}$
$^4F_{7/2}$	37	13 287	4,5	13 280	4,5	90.5 $^4F_{7/2}$+3.21 $^4S_{3/2}$+2.83 $^4F_{5/2}$
(13 466)	38	13 320	4,5	13 323	4,5	94.8 $^4S_{3/2}$+3.93 $^4F_{7/2}$+0.44 $^4G_{5/2}$
	39	13 353	6	13 351	6	94.8 $^4S_{3/2}$+4.15 $^4F_{7/2}$+0.18 $^4G_{5/2}$
$^4S_{3/2}$	40	13 499	6	13 504	6	91.8 $^4F_{7/2}$+4.36 $^4S_{3/2}$+1.21 $^2H_{9/2}$
	41	13 514	4,5	13 512	4,5	95.2 $^4F_{7/2}$+2.44 $^4F_{5/2}$+1.03 $^4F_{9/2}$
(13 346)	42	⋯	4,5	13 610	4,5	93.9 $^4F_{7/2}$+3.30 $^4F_{9/2}$+1.76 $^4F_{5/2}$
$^4F_{9/2}$	43	14 687	4,5	14 687	4,5	97.3 $^4F_{9/2}$+0.81 $^2H_{11/2}$+0.57 $^4F_{7/2}$
	44	14 755	4,5	14 754	4,5	95.1 $^4F_{9/2}$+3.55 $^4F_{7/2}$+0.64 $^2H_{11/2}$
(14 797)	45	14 763	6	14 765	6	98.0 $^4F_{9/2}$+0.79 $^4F_{7/2}$+0.37 $^4F_{5/2}$
	46	14 837	4,5	14 833	4,5	98.3 $^4F_{9/2}$+0.83 $^4F_{7/2}$+0.28 $^2G_{7/2}$
	47	15 058	6	15 055	6	99.2 $^4F_{9/2}$+0.23 $^2G_{7/2}$+0.21 $^2H_{9/2}$
$^2H_{11/2}$	48	⋯	4,5	16 051	4,5	98.3 $^2H_{11/2}$+1.09 $^2G_{7/2}$+0.14 $^4F_{7/2}$
(16 101)	49	16 067	6	16 063	6	98.9 $^2H_{11/2}$+0.76 $^2G_{7/2}$+0.10 $^4F_{7/2}$
	50	16 086	4,5	16 092	4,5	97.7 $^2H_{11/2}$+1.68 $^2G_{7/2}$+0.34 $^4F_{9/2}$
	51	16 119	6	16 106	6	98.8 $^2H_{11/2}$+0.39 $^2G_{7/2}$+0.39 $^4F_{9/2}$
	52	16 130	4,5	16 134	4,5	98.6 $^2H_{11/2}$+0.66 $^4F_{9/2}$+0.31 $^2H_{9/2}$
	53	16 165	4,5	16 189	6	99.2 $^2H_{11/2}$+0.37 $^4F_{9/2}$+0.29 $^2G_{7/2}$
$^4G_{5/2}$	54	17 071	4,5	17 070	4,5	83.1 $^4G_{5/2}$+15.3 $^2G_{7/2}$+0.38 $^4S_{3/2}$
(17 291)	55	17 192	4,5	17 193	4,5	75.7 $^4G_{5/2}$+23.3 $^2G_{7/2}$+0.42 $^2H_{11/2}$
	56	17 345	6	17 349	6	67.8 $^2G_{7/2}$+30.5 $^4G_{5/2}$+0.84 $^2H_{11/2}$

TABLE V. (*Continued.*)

$^{2S+1}L_J$[a]	Level	E (cm^{-1})[b] (expt.)	Γ_n[c] (expt.)	E (cm^{-1})[b] (calc.)	Γ_n[d] (calc.)	Free-ion percent mixture
$^2G_{7/2}$	57	17 525	4,5	17 528	4,5	$97.4\ ^2G_{7/2}+1.02\ ^2H_{11/2}+0.97\ ^4G_{5/2}$
(17 459)	58	17 600	4,5	17 596	4,5	$84.2\ ^2G_{7/2}+14.6\ ^4G_{5/2}+0.39\ ^2H_{11/2}$
	59	17 661	4,5	17 653	4,5	$74.3\ ^2G_{7/2}+23.5\ ^4G_{5/2}+1.11\ ^2H_{11/2}$
	60	⋯	6	17 681	6	$68.3\ ^4G_{5/2}+30.3\ ^2G_{7/2}+0.44\ ^2H_{11/2}$

[a]Multiplet manifold of Nd^{3+} ($4f^3$); the centroid in parentheses is given in cm^{-1}.
[b]Experimental levels taken from Table I.
[c]Assignments based on selection rules for C_3 symmetry assuming the ground-state level is $\Gamma_{4,5}$.
[d]Calculated splitting and predicted symmetry labels ($\Gamma_{4,5}$ or Γ_6) based on B_{nm} parameters reported in Table VI.

B_{nm} parameters are necessary to obtain a final rms value of 6 cm^{-1} between 46 calculated and experimental levels. Overall agreement suggests that the lattice-sum model is appropriate for describing those Nd^{3+} ions in one of the nonfluorescing sites in Nd:FAP. We were not able to obtain sufficient data sets to articulate other sites. The fact that we observed no conclusive hot band data in absorption is not contradicted by the predicted splitting of $^4I_{9/2}$. For Nd^{3+} ions that occupy this site, transitions from a Stark level 270 cm^{-1} above the ground state would very likely be too weak and broad to observe even at room temperature.

In conclusion, site-selective spectroscopy has permitted differentiation between Nd^{3+} ions in multiple sites in the fluorapatite crystals Nd:SFAP and Nd:FAP. Attempts to refine the point-charge lattice-sum model are ongoing in hopes of obtaining improved understanding of the complex nature of charge compensation associated with heterovalent substitution of R^{3+} ions in crystals with the fluorapatite structure.[24,27]

TABLE VI. Crystal-field parameters for Nd^{3+} ions in C_3 sites in Nd:FAP.

B_{nm} parameter	Lattice sum[a] (cm^{-1})	Final set[b] (cm^{-1})
B_{20}	1247	1251
B_{40}	−2252	−2518
B_{43}	1016	605
B_{60}	−1176	−1237
Re B_{63}	890	899
$I_m B_{63}$	−260	−126
Re B_{66}	−117	−14.6
$I_m B_{66}$	356	474
$I_2(B)$[c]	1247	
$I_4(B)$	2671	
$I_6(B)$	1544	

[a]Charge on oxygen taken as −1.8, phosphorus +4.2, in electron charge units; x-ray crystallography data taken from Ref. 22 for symmetry properties and bond distances; for details regarding calculations see Ref. 35.
[b]Since fluorescence is not observed, fitting analysis involved 14 multiplet manifolds higher in energy than the $^4I_{9/2}$ and $^4I_{11/2}$; original estimates for the centroids of $^4I_{9/2}$ and $^4I_{11/2}$ were taken from Table III.
[c]Rotational invariants, $I_n(B)$, are in units of cm^{-1} (Ref. 31).

ACKNOWLEDGMENTS

The authors wish to thank Professor R. E. Peale (Department of Physics, University of Central Florida, Orlando, FL) for allowing us to compare our independent results with his, and Dr. B. Zandi (U.S. Army Research Laboratory, Ft. Belvoir, VA) for checking the results of our crystal-field splitting calculations.

[1] B. H. T. Chai, in *Novel Laser Sources and Applications*, edited by J. F. Becker, A. C. Tam, J. B. Gruber, and L. Lam (SPIE, Bellingham, WA, 1994), p. 5.
[2] J. B. Gruber, J. A. Hutchinson, D. C. Harris, M. D. Seltzer, T. H. Allik, C. A. Morrison, and M. P. Scripsick, in *Materials Research Society Symposium Proceedings*, edited by B. H. T. Chai, S. A. Payne, T. Y. Fan, and T. H. Allik (Materials Research Society, Pittsburgh, PA, 1994), Vol. 329, p. 209.
[3] L. D. De Loach, S. A. Payne, L. L. Chase, L. K. Smith, W. L. Kway, and W. F. Krupke, IEEE J. Quantum Electron. **QE-29**, 1179 (1993).
[4] S. A. Payne, L. K. Smith, L. D. De Loach, W. L. Kway, J. B. Tassano, and W. F. Krupke, IEEE J. Quantum Electron. **QE-31**, 412 (1993); see also S. A. Payne, W. F. Krupke, L. K. Smith, L. D. De Loach, and W. L. Kway, in *OSA Proceedings on Advanced Solid-State Lasers*, edited by L. L. Chase and A. A. Pinto (Optical Society of America, Washington DC, 1992), Vol. 13, p. 227.
[5] R. E. Peale, P. L. Summers, H. Weidner, B. H. T. Chai, and C. A. Morrison, J. Appl. Phys. **77**, 270 (1995).
[6] A. O. Wright, M. D. Seltzer, J. B. Gruber, and B. H. T. Chai, J. Appl. Phys. (to be published).
[7] A. O. Wright, M. D. Seltzer, J. B. Gruber, B. Zandi, L. D. Merkle, and B. H. T. Chai (unpublished).
[8] P. Hong, X. X. Zhang, R. E. Peale, H. Weidner, M. Bass, and B. H. T. Chai, J. Appl. Phys. **77**, 294 (1995).
[9] L. D. De Loach, S. A. Payne, W. L. Kway, J. B. Tassano, S. N. Dixit, and W. F. Krupke, J. Lumin. **62**, 85 (1994).
[10] T. H. Allik, J. B. Gruber, M. D. Seltzer, M. E. Hills, K. Spariosu, R. D. Stultz, M. Birnbaum, C. A. Morrison, B. H. T. Chai, J. A. Hutchinson, and L. D. Merkle, in *OSA Proceedings on Advanced Solid-State Lasers*, edited by L. L. Chase and A. A. Pinto (Optical Society of America, Washington DC, 1993), Vol. 15, p. 246.
[11] J. B. Gruber, M. D. Seltzer, M. E. Hills, T. H. Allik, J. A. Hutchinson, C. A. Morrison, and B. H. T. Chai, Opt. Mater. **3**, 99 (1994).
[12] K. Spariosu, R. D. Stultz, M. Birnbaum, T. H. Allik, and J. A. Hutchinson, Appl. Phys. Lett. **62**, 2763 (1993).
[13] R. C. Ohlmann, K. B. Steinbruegge, and R. Mazelsky, Appl. Opt. **7**, 905 (1968).
[14] R. Mazelsky, R. C. Ohlmann, and K. Steinbruegge, J. Electrochem. Soc. Solid State Sci. **115**, 68 (1968).
[15] G. V. Maksimova and A. A. Sobol', Inorg. Mater. **8**, 945 (1972).
[16] G. V. Maksimova and A. A. Sobol', Tr. Fiz. Inst. Akad. Nauk. **60**, 55 (1972).
[17] K. B. Steinbruegge, T. Henningsin, R. H. Hopkins, R. Mazelsky, N. T. Melamed, E. P. Riedel, and G. W. Roland, Appl. Opt. **11**, 999 (1972).
[18] F. M. Ryan, R. W. Warren, R. H. Hopkins, and J. Murphy, J. Electrochem. Soc. Solid State Sci. **125**, 1493 (1978).

[19] J. B. Gruber, C. A. Morrison, D. C. Harris, M. D. Seltzer, T. H. Allik, J. A. Hutchinson, and M. P. Scripsick, J. Appl. Phys. **77**, 4321 (1995).
[20] St. Naray-Szabo, Z. Kristallogr. **75**, 387 (1930).
[21] R. W. Wyckoff, Cryst. Struct. **3**, 228 (1965).
[22] J. M. Hughes, M. Cameron, and K. D. Crowley, Am. Mineral. **74**, 870 (1989).
[23] M. E. Fleet and Y.-M. Pan, J. Solid State Chem. **112**, 78 (1994).
[24] J. B. Gruber, *Tunable Lasers for Engineering and Biological Applications* (SPIE, Bellingham, WA, 1992).
[25] G. V. Maksimova and A. A. Sobol', Proc. P. N. Lebedev Phys. Inst. **60**, 59 (1974).
[26] M. Greenblatt and J. H. Pifer, J. Chem. Phys. **66**, 559 (1977).
[27] C. A. Morrison, Army Research Laboratory, Report ARL-TR-708, Adelphi, MD, April, 1995.
[28] H. A. Bethe, Ann. Phys. (Leipzig) **3**, 133 (1929).
[29] J. L. Prather, *Atomic Energy Levels in Crystals*, NBS Monograph 19 (U.S. Department of Commerce, National Bureau of Standards, Washington DC, 1961).
[30] W. T. Carnall, P. R. Fields, and K. Rajnak, J. Chem Phys. **49**, 4412 (1968); **49**, 4424 (1968); **49**, 4443 (1968); **49**, 4447 (1968); **49**, 4450 (1968).
[31] C. A. Morrison and R. P. Leavitt, J. Chem. Phys. **71**, 2366 (1979).
[32] N. C. Chang, J. B. Gruber, R. P. Leavitt, and C. A. Morrison, J. Chem. Phys. **76**, 3877 (1982).
[33] J. B. Gruber, R. P. Leavitt, C. A. Morrison, and N. C. Chang, J. Chem. Phys. **82**, 5373 (1985).
[34] C. A. Morrison and R. P. Leavitt, in *Handbook of the Physics and Chemistry of Rare Earths*, edited by K. Gschneidner, Jr., and L. Eyring (North-Holland, New York, 1982), Vol. 5, p. 461.
[35] R. P. Leavitt, C. A. Morrison, and D. E. Wortman, *Three Parameter Theory of Crystal Fields*, HDL-TR-1673 (June 1975); NTIS No. ADA017849 (U.S. Army Research Laboratory, Adelphi, MD, 1975).
[36] C. A. Morrison, *Angular Momentum Theory Applied to Interactions in Solids, Lecture Notes in Chemistry*, No. 47 (Springer, New York, 1988); a discussion on the reduction of the number of independent B_{nm} by rotation is given on pp. 86–87.